Automatic detection of welding defects using texture features

Domingo Mery and Miguel Angel Berti
Departamento de Ingeniería Informática
Universidad de Santiago de Chile
Av. Ecuador 3659, Santiago de Chile
EMail: dmery@ieee.org, miguel.berti@usach.cl
http://www.diinf.usach.cl/~dmery

ABSTRACT

In this paper we present a new approach to detecting weld defects from digitalised films based on texture features. Texture is one of the most important features used in recognising patterns in an image. However, these features are not yet commonly exploited in the analysis of X-ray images in NDT. The paper describes two groups of widely used texture features: 1) features based on the co-occurrence matrix, which gives a measurement of how often one grey value will appear in a specified spatial relationship to another grey value on the image; and 2) features based on 2D Gabor functions, i.e., Gaussian shaped band-pass filters, with dyadic treatment of the radial spatial frequency range and multiple orientations, which represent an appropriate choice for tasks requiring simultaneous measurement in both space and frequency domains. The proposed approach to detecting weld defects follows a general pattern recognition scheme based on three steps: segmentation, feature extraction and classification. That is, in our case, 1) potential defects are segmented using an edge detector based on the Laplacian-of-Gauss operator; 2) texture features of the potential defects are extracted; and 3) the most relevant features are used as input data on a statistical classifier. This preliminary study makes a contribution to the improvement of the automatic detection of welding defects.

1. Introduction

As illustrated in Fig. (1), the methodology used in this investigation follows the pattern recognition schema: image segmentation, feature extraction and classification (Castleman, 1996; Mery et al, 2003). The segmentation process oriented towards the detection of edges by employing the LoG filter (Mery & Filbert, 2002). This technique searches for changes in the grey values of the image (edges) thus identifying zones delimited by edges that indicate flaws. The segmentation detects regions that are denominated as 'hypothetical defects'. However, only some of them are defects and the others are false alarms. Subsequently, the *feature extraction* is centred principally on the measurement of properties of the regions. Finally, *classification* orders segmented regions in specific regions according to extracted features, assigning each region to one of a number of pre-established groups, which represent all possible types of regions expected in the image. We will differentiate between the *detection of defects* and the *classification of defects* (Liao, 2003). In the detection problem, the classes that exist are only two: 'defects' or 'no defects', whereas the recognition of the type of the defects (e.g., porosity, slag, crack, lack of penetration, etc.) is known as classification of flaws types. In this paper, we study some texture features in order to *detect* the defects present in welding seams.

The paper is organised as follows. Section 2 briefly gives an overview of the existing methods automatic detection or classification of welding defects. Section 3 presents the texture features used in our investigation. Section 4 carries out a feature selection in order to reduce computational cost of classification. In Section 5, the experiments and the results obtained by using statistical classifiers are shown. Finally, our conclusions are presented.

2. State of the art

In this Section we present several methods that have been published in the last 15 years that perform an automatic detection or classification of welding defects.

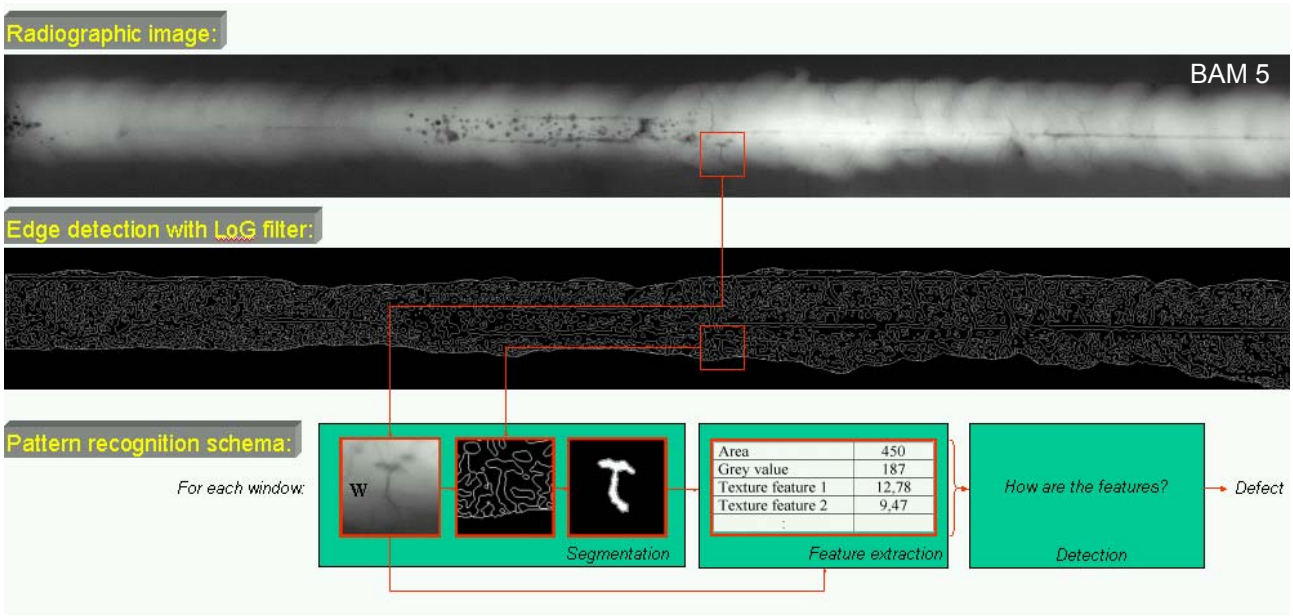

Fig. 1: Detection of welding defects using a pattern recognition schema.

2.1 Gayer et al.'s Method

The proposed method (Gayer et al, 1990) can be summarized as having two steps:

i) A quick search for potential defects in the X-ray image: Assuming that the defects will be smaller than the regular structure of the test piece, potential defects are classified as those regions of the image where higher frequencies are significant. The spectrum of the X-ray image is determined with the help of a fast Fourier transformation, which is calculated either row by row or column by column in little 32×32 windows. When the sum of the higher frequencies of a window is greater than a given threshold value, the entire window is marked as potentially defective. Another possibility is suggested by the authors as part of this task: A window is selected as potentially defective when the sum of the first derivative of the rows and columns of a window is large enough.

ii) Identification and location of the true defect: Because of the time consuming nature of this step, only those regions, which were previously classified as being potentially defective, are studied here. Two algorithms were developed here as well. The first leads to a matching[1] between the potential defect and typical defects, which are stored in a library as templates. Whenever a large resemblance between the potential defect and a template is found, the potential defect is classified as a true defect. The second algorithm estimates a defect-free X-ray image of the test piece by modelling every line of an interpolated spline function without special consideration for the potentially defective region. Following this, the original and the defect-free images are compared. True defects are identified when large difference occurs compared to the original input image.

2.2 Lawson and Parker's Method

In 1994 Lawson and Parker proposed in (Lawson & Parker, 1994) that artificial neural networks (ANN) be used for the automated detection of defects in X-ray images. The method generates a binary image from the test image where each pixel is either 0 when a regular structure feature of the piece or 1 when a defect is detected. This entails the supervised learning of a multi-layer perceptron network (MLP) where the attempt is made to obtain detection from training data. A back propagation algorithm is used for the assignment of weightings within the MLP.

The authors use one of two hidden layers in the network topography of the ANN, where the input signal corresponds to a window of $m \times m$ grey values in the X-ray image. The output signal is the

[1] Matching is performed with a Sequential Similarity Detection method.

pixel at the image centre in the binary image. Since the threshold value function for the neurons are sigmoidal in this method, a threshold is used to obtain a binary output signal.

The desired detection in the training data was obtained with a segmenting procedure based on an adaptive threshold. During the experiments of five X-ray images, Lawson and Parker show that the detection using ANN is superior to the segmenting method using adapted thresholds.

2.3 Defect recognition using shape features

A method for automated recognition of welding defects was presented in (Sofia & Redouane, 2002). The detection follows a pattern recognition methodology: i) Segmentation: regions of pixels are found and isolated from the rest of the X-ray image using a watershed algorithm and morphological operations (erosion and dilation). ii) Feature extraction: the regions are measured and shape characteristics (diameter variation and main direction of inertia based on invariant moments) are quantified. iii) Classification: the extracted features of each region are analysed and classified using a *k*-nearest neighbour classifier. According to the authors, the method is robust and achieves a good detection rate.

2.4 Defect recognition using linear classifiers

In (Silva et al, 2002) a method to welding defect classification is proposed. In a first step, called image pre-processing, the quality of the X-ray image is improved using a median filter and a contrast enhancement technique. The defect detection follows the pattern recognition schema mentioned above: i) Potential defects are segmented in the X-ray image. ii) Geometric and grey value features (contrast (*C*), position (*P*) , aspect ratio (*a*), width-area ratio (*e/A*), length-area ratio (*L/A*) and roundness(*R*)) are extracted. The correlation between features and each considered defect class (slag inclusion, porosity, lack of penetration and undercutting) was evaluated by analysing the linear correlation coefficient. iii) The most relevant features were used as input data on a hierarchic linear classifier (Silva et al, 2001).

In order to achieve a higher degree of reliability for the results, radiographic standards from International Institute of Welding were used, with 86 films containing the main defect classes. The experimental results shown that the features *P* and *e/A* are able to classify the classes undercutting and lack of penetration. Nevertheless, the six mentioned features are required to obtain a high performance by classifying the porosity and inclusion defects.

2.5 Background subtraction method

Liao and Li (1998) propose a detection approach based on a curve fitting. The key idea of this work is to simulate a 2D background of a normal welding bead characterised by low spatial frequencies in comparison with the high spatial frequencies of image of the defects. Thus, a 2D background is estimated by fitting each vertical line of the weld to a polynomial function. Thus, the obtained image is subtracted from the original image. The defects are detected where the difference is considerable. Wang & Liao (2002) and Liao (2003) propose a fuzzy *k*-nearest neighbour, multi-layer perceptron neural network and a fuzzy expert system for the classification welding defect types. The features used for the classification are distance from centre, circularities, compactness, major axis, width and length, elongation, Heywood diameter and average intensity and standard deviation of intensity.

In this literature review, we observe that usually features that provide information about the grey values (intensity features) are used to detect the flaws, whereas geometric features are employed to classify them.

3. Texture features

Texture is one of the most important features used in recognising patterns in an image. However, these features are not yet commonly exploited in the analysis of X-ray images in NDT (see literature review in Section 2). In this Section, we describe two groups of widely used texture features: 1) features based on the co-occurrence matrix, and 2) features based on 2D Gabor functions. Once the X-ray image is segmented, the edge detection provides windows (see for

example window **W** in Fig. (1)) which texture features can be extracted. Each window **W** is defined as the rectangle that includes the segmented hypothetical defect and its surroundings.

3.1 Texture features based on co-occurrence matrix

These features give a measurement of how often one grey value will appear in a specified spatial relationship to another grey value on the image. We use, in this case, the pixels of each window **W** that contains the hypothetical defect and its surrounding (see Fig. (1)).

The co-occurrence matrix $\mathbf{P}_{kl}$ (Castleman, 1996; Haralick et al, 1973) is defined as follows. The element $P_{kl}(i,j)$ of this matrix for a window is the number of times, divided by N_T, that grey-levels i and j occur in two pixels separated by that distance and direction given by the vector (k,l) or (-k,-l), where N_T is the number of pixels pairs contributing to $\mathbf{P}_{kl}$. In order to decrease the size $N_x \times N_x$ of the co-occurrence matrix the grey scale is often reduced from 256 to 8 grey levels. From the co-occurrence matrix several texture features can be computed. The 14 Haralick features (Haralick et al, 1973) are defined as follows for $p(i,j) := P_{kl}(i,j)$:

angular second moment

$$f_1 = \sum_{i=1}^{N_x}\sum_{j=1}^{N_x}\left[p(i,j)\right]^2 \tag{1}$$

contrast

$$f_2 = \sum_{n=0}^{N_x-1} n^2 \sum_{i=1}^{N_x}\sum_{\substack{j=1 \\ |i-j|=n}}^{N_x} p(i,j) \tag{2}$$

correlation

$$f_3 = \frac{1}{\sigma_x \sigma_y}\sum_{i=1}^{N_x}\sum_{j=1}^{N_x}(ij \cdot p(i,j) - \mu_x \mu_y)^2 \tag{3}$$

sum of squares

$$f_4 = \sum_{i=1}^{N_x}\sum_{j=1}^{N_x}(i-j)^2\, p(i,j) \tag{4}$$

inverse difference moment

$$f_5 = \sum_{i=1}^{N_x}\sum_{j=1}^{N_x}\frac{1}{1+(i-j)^2}\, p(i,j) \tag{5}$$

sum average

$$f_6 = \sum_{i=2}^{2N_x} i \cdot p_{x+y}(i) \tag{6}$$

sum variance

$$f_7 = \sum_{i=2}^{2N_x}(i - f_8)\, p_{x+y}(i) \tag{7}$$

sum entropy

$$f_8 = -\sum_{i=2}^{2N_x} p_{x+y}(i)\log\left[p_{x+y}(i)\right] \tag{8}$$

entropy

$$f_9 = -\sum_{i=1}^{N_x}\sum_{j=1}^{N_x} p(i,j)\log\left[p(i,j)\right] \tag{9}$$

difference variance

$$f_{10} = \mathrm{var}(\mathbf{p}_{x+y}) \tag{10}$$

difference entropy

$$f_{11} = -\sum_{i=0}^{N_x-1} p_{x-y}(i)\log\left[p_{x-y}(i)\right] \tag{11}$$

information measures of correlation 1

$$f_{12} = \frac{f_9 - HXY1}{\max(HX, HY)} \tag{12}$$

information measures of correlation 2

$$f_{13} = \sqrt{1-\exp\left[-2(HXY2 - HXY)\right]} \tag{13}$$

maximal correlation coefficient

$$f_{14} = \sqrt{\lambda_2} \tag{14}$$

where μ_x, μ_y, σ_x and σ_y are the means and standard deviations of p_x and p_y respectively, and

$$p_x = \sum_{j=1}^{N_x} p(i,j), \quad p_y = \sum_{i=1}^{N_x} p(i,j),$$

$$HX = -\sum_{i=1}^{N_x} p_x(i)\log[p_x(i)]$$

$$HY = -\sum_{j=1}^{N_x} p_y(j)\log[p_y(j)]$$

$$p_{x+y}(k) = \sum_{i=1}^{N_x}\sum_{\substack{j=1 \\ i+j=k}}^{N_x} p(i,j) \quad k = 2,3,...,2N_x.$$

$$HXY1 = -\sum_{i=1}^{N_x}\sum_{j=1}^{N_x} p(i,j)\log[p_x(i)p_y(j)]$$

$$HXY2 = -\sum_{i=1}^{N_x}\sum_{j=1}^{N_x} p_x(i)p_y(j)\log[p_x(i)p_y(j)]$$

$$p_{x-y}(k) = \sum_{i=1}^{N_x}\sum_{\substack{j=1 \\ |i-j|=k}}^{N_x} p(i,j) \quad k = 0,3,...,N_x\text{-}1.$$

λ_2 is the second largest eigenvalue of Q

$$Q(i,j) = \sum_{k=1}^{N_x} \frac{p(i,k)p(j,k)}{p_x(i)p_y(k)}$$

The texture features are extracted for four directions (0º-180º, 45º-225º, 90º-270º and 135º-315º) in different distances d =max(k,l), i.e., for a given distance d we have four possible co-occurrence matrices: $\mathbf{P}_{0d}$, $\mathbf{P}_{dd}$, $\mathbf{P}_{d0}$ and $\mathbf{P}_{-dd}$. For example for d = 1, we have (k,l) = (0,1); (1,1); (1,0); and (-1,1). After Haralick, et al (1973), 14 textures features using each co-occurrence matrix are computed, and the mean and range for each feature are calculated, i.e., we obtain 14 × 2 = 28 texture features for each distance d. The features will be denoted as f'_i for the mean and f''_i for the range, for i = 1,..., 14.

3.2 Texture features based on Gabor functions

The Gabor functions are Gaussian shaped band-pass filters, with dyadic treatment of the radial spatial frequency range and multiple orientations, which represent an appropriate choice for tasks requiring simultaneous measurement in both space and frequency domains. The Gabor functions are a complete (but a nonorthogonal) basis set given by:

$$f(x,y) = \frac{1}{2\pi\sigma_x\sigma_y}\exp\left(-\frac{1}{2}\left(\frac{x^2}{\sigma_x^2}+\frac{y^2}{\sigma_y^2}\right)\right)\exp(2\pi j u_0 x), \tag{15}$$

where σ_x and σ_y denote the Gaussian envelope along the x and y-axes, and u_0 defines the radial frequency of the Gabor function. Examples of Gabor functions are illustrated in Fig. (2). In this case a class of self-similar functions are generated by rotation and dilation of $f(x,y)$.

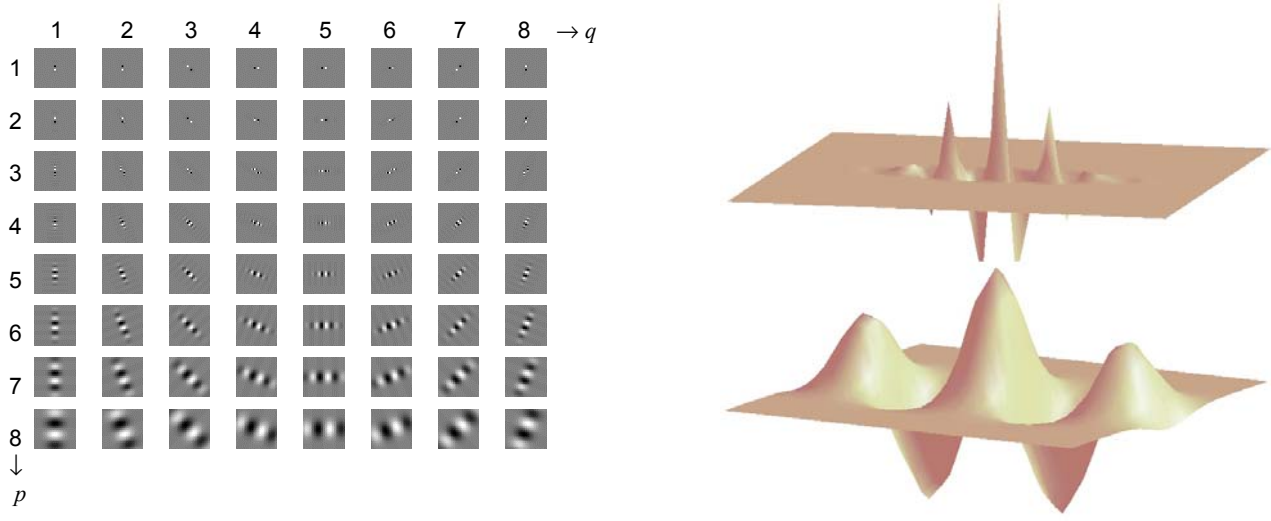

(a) (b)

Fig. 2: Example of Gabor functions in spatial domain: a) imaginary components of self-similar filter bank by using p = 1,..., 8 scales and q = 1,..., 8 orientations, b) 3D representations of two functions of a).

Each Gabor filter has a real and an imaginary component that are stored in $M \times M$ masks, called $\mathbf{R}_{pq}$ and $\mathbf{I}_{pq}$ respectively, where $p = 1, ..., S$, denotes the scale, and $q = 1, ..., L$, denotes the orientation (for details see (Kumar & Pang, 2002)). In our work we use $S = 8$ scales, and $L = 8$ orientations as shown in Fig. (2), with $M = 27$.

The Gabor filters are applied to each segmented windows **W** that contains the hypothetical defect and its surrounding (see Fig. (1)). The filtered windows $\mathbf{G}_{pq}$ are computed using the 2D convolution of the window **W** of the X-ray image with the Gabor masks as follows:

$$\mathbf{G}_{pq} = [\ (\mathbf{W} * \mathbf{R}_{pq})^2 + (\mathbf{W} * \mathbf{I}_{pq})^2\ ]^{1/2}, \tag{16}$$

where $*$ denotes the 2D convolution operation. The Gabor features, denoted by g_{pq}, are defined as the average output of $\mathbf{G}_{pq}$, i.e., it yields $S \times L$ Gabor features for each segmented window:

$$g_{pq} = \frac{1}{n_w m_w} \sum_{i=1}^{n_w} \sum_{j=1}^{m_w} G_{pq}(i, j) \tag{17}$$

where the size of the filtered windows $\mathbf{G}_{pq}$ is $n_w \times m_w$.

4. Feature Selection

In this work, 28 texture features based on co-occurrence matrix for 3 distances, and 64 texture features based on Gabor functions were extracted. That is, there are $28 \times 3 + 64 = 148$ extracted features for each segmented region.

The ROC (*receiver operation characteristic*) analysis is commonly used to measure the performance of a two-class classification. In our case, each feature is analysed independently using a threshold classifier. This way, a hypothetical flaw is classified as a 'no-defect' (or 'defect') if the value of the feature is below (or above) a threshold value. The ROC curve represents a 'sensitivity' (S_n) versus '1-specificity' ($1\text{-}S_p$), defined as:

$$S_n = \frac{TP}{TP + FN}, \qquad 1 - S_p = \frac{FP}{TN + FP} \tag{18}$$

in which TP is the number of true positives (correctly detected defects), TN is the number of true negatives (correctly detected no-defects), FP is the number of false positives (false alarms, or no-defects detected as defects) and FN false negatives (flaws detected as no-defects). Ideally, $S_n = 1$ and $1\text{-}S_p = 0$, this means that all defects were found without any false alarms. The ROC curve makes it possible to evaluate the performance of the detection process at different points of operation (as defined for example by means of classification thresholds). The area under the curve (A_z) is normally used as a measure of this performance as it indicates how flaw detection can be carried out: a value of $A_z = 1$ indicates an ideal detection, while a value of $A_z = 0.5$ corresponds to random classification (Egan, 1975).

In order to reduce the computational time required for classification it is necessary to select features; this way the classifier only works with non-correlated features that provide flaw detection information. There are a variety of methods for evaluating the performance of the extracted features. The present Section includes only the *Sequential Forward Selection* (SFS) method (Jain, et al, 2000). This method requires an objective function J obtained from the Fisher discriminant (Fukunaga, 1990) that evaluates the performance of the classification using m features. The method begins with one feature (m =1), and a search is performed for the feature that maximises the function J. Subsequently, a second search is carried out for that feature that maximises the function J with two features (m =2). This method ensures that neither features that are correlated with the already selected feature nor those that do not maximise f are considered. This process is repeated until the best n features are obtained. This approach works best with normalised features, i.e., those that have been linearly transformed in such a way as to obtain a mean value equal to zero, and a variance equal to one.

5. Experiments and results

The X-ray image BAM-5, shown in Fig. (1), was analysed. The size of the image is 3.512 × 366 pixels. After the segmentation step, 1.419 hypothetical defects were obtained. According to a human visual inspection, in the segmented regions only 198 were defects. Nevertheless, the segmentation process could detect all defects bigger than 15 pixels. The 28 × 3 texture features based on co-occurrence matrix and the 64 texture features based on Gabor functions were extracted for each of the 1.419 segmented hypothetical defect.

Table (1) presents the top ten values obtained by computing the area under the ROC curve (A_z) and the Fisher discriminant (J) in our data. The best texture features based on the co-occurrence matrix are the mean of the difference entropy and the mean of the difference variance (equations (8) and (7) respectively), for the distances d = 3, 2, 1. In the other hand, the best Gabor features are at p = 6 (scale) and the orientations: ↘, —, and ↗. The ROC and the class distribution of feature $f'_{11}@\ d$=3 is shown in Fig. (3).

The results obtained by the features selection based on the SFS method are shown in Fig. (4) for the first seven features. We observe that only one Gabor feature was selected. The feature space is illustrated in Fig. (5) for the first three selected features. The figure shows that the class 'defect' and 'no-defect' are good separable in the extreme. In the middle, the two classes are mixed.

Table 1: ROC analysis and Fisher discriminant

Feature	A_z
g_{63}	0.9287
$f'_{11}@\ d$=3	0.9285
$f'_{10}@\ d$=3	0.9207
g_{65}	0.9178
g_{67}	0.9124
$f'_{11}@\ d$=2	0.8969
$f'_{10}@\ d$=2	0.8620
g_{57}	0.8600
$f'_{2}@\ d$=3	0.8523
$f'_{2}@\ d$=2	0.8474

Feature	J
$f'_{11}@\ d$=3	1.1376
$f'_{10}@\ d$=3	1.0496
g_{63}	0.9132
g_{67}	0.8997
$f'_{11}@\ d$=2	0.8948
$f'_{10}@\ d$=2	0.7638
$f'_{11}@\ d$=1	0.6936
$f'_{10}@\ d$=1	0.6700
g_{65}	0.6525
$f'_{5}@\ d$=1	0.5998

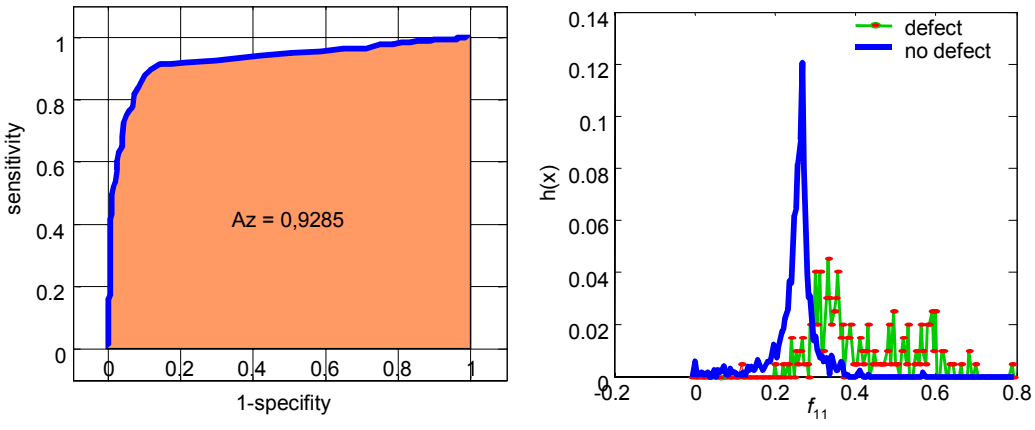

Fig. 3: ROC and class distribution of feature $f'_{11}@\ d$=3

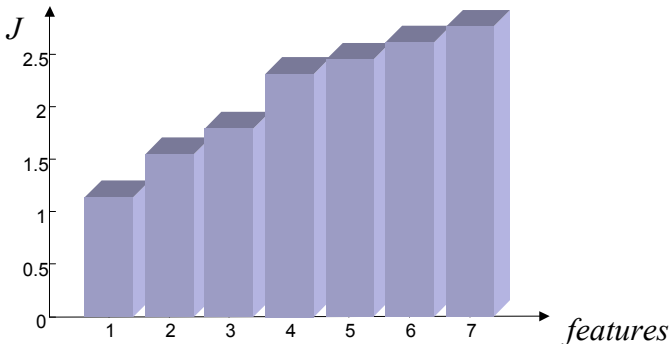

Fig. 4: SFS method: the selected features are: 1) f'_{11}@ d=3; 2) f'_{11}@ d=2; 3) f''_{10}@ d=3; 4) f'_{10}@ d=2; 5) f''_{11}@ d=3; 6) f'_5@ d=1; and 7) g_{63}.

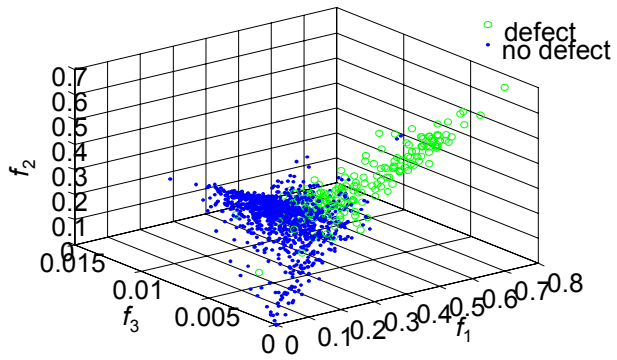

Fig. 5: Feature space for the first three selected features: 1) $f_1 = f'_{11}$@ d=3; 2) $f_2 = f'_{11}$@ d=2; 3) $f_3 = f''_{10}$@ d=3.

Table 2: Detection performance

Detector	***TP***	***FP***	***FN***	***TN***	S_n	1-S_p
Ideal	198	0	0	1221	100,0%	0,0%
Polynomial	180	99	18	1122	90,91%	8,11%
Mahalanobis	180	155	18	1066	90,91%	12,69%
nearest neighbour	157	168	41	1053	79,29%	13,75%

Finally, we present the results obtained by a statistical classifications with the seven selected features. In these experiments, we use the polynomial, Mahalanobis and nearest neighbour classifiers (Mery et al, 2003). The results are summarised in Table (2), where the true positives, false positives, false negatives, true negatives, sensibility, and 1-specificity are tabulated for the ideal detector and the mentioned classifiers. The best performance is obtained by the polynomial classifier, where fast 91% of the existing flaws were detected with 8% of false alarms.

6. Conclusions

In this paper we presented a new approach to detecting weld defects based on two groups of widely used texture features: 1) features based on the co-occurrence matrix, and 2) features based on 2D Gabor functions. The best texture features based on the co-occurrence matrix are the mean of the difference entropy and the mean of the difference variance, for a distance of d = 3. In the other and, the best Gabor features are at p = 6 (scale) and the orientations: ↘, —, and ↗. The area under the ROC curve for these cases is about A_z = 0,92. The best performance is obtained by the polynomial classifier, fast 91% of the existing flaws were detected with 8% of false alarms. This preliminary study makes a contribution to the improvement of the automatic detection of welding defects.

Acknowledgements

The authors wish to thank the Department for Research and Development of the Universidad de Santiago de Chile (project DICYT 06-0119MQ) for financing this investigation, and the Technical University of Berlin for financing the participation in this Symposium. The authors would like to thank the Federal Institute for Materials Research and Testing (BAM) in Berlin for the radiographic material.

References

Castleman, K.R. (1996). *Digital Image Processing*, Prentice-Hall, New Jersey.

Ditchburn, R.; Burke, S.; Scala M. (1996). NDT of Welds: State of the Art. *NDT&E International*, 29(2):111-117.

Fukunaga, K., 1990, *Introduction to statistical pattern recognition*, Academic Press, Inc., Second Edition, San Diego.

Gayer, A.; Saya, A.; Shiloh, A. (1990). Automatic recognition of welding defects in real-time radiography. *NDT International*, 23(4):131–136.

Haralick, R.; Shanmugam, K.; Dinstein, I. (1973). Textural Features for Image Classification. *IEEE Transaction on Systems, Man, Cybernetics*, SMC-3(6):610-621.

Kumar, A., Pang, G.K.H, 2002: Defect Detection in Textured Materials Using Gabor Filters. *IEEE Transactions on Industry Applications*, 38(2):425-440.

Lawson, S.W.; Parker, G.A. (1994). Intelligent segmentation of industrial radiographic images using neural networks. In *Machine Vision Applications and Systems Integration III, Proc. of SPIE*, volume 2347, pages 245–255, November 1994.

Liao, T.W.; Ni, J. (1996). An Automated Radiographic NDT System for Weld Inspection: Part I – Weld Extraction. *NDT&E International*, 29(3):157-162.

Liao, T.W.; Li, Y.M.. (1998). An Automated Radiographic NDT System for Weld Inspection: Part II – Flaw detection. *NDT&E International*, 31(3):183-192.

Liao, T.W. (2003): Classification of welding flaw types with fuzzy expert systems. *Expert Systems with Applications*, 25(2003): 101-111.

Mery, D., Filbert, D., 2002, Automated Flaw Detection in Aluminum Castings Based on the Tracking of Potential Defects in a Radioscopic Image Sequence. *IEEE Transactions on Robotics and Automation*, 18(6): 890-901.

Mery, D., da Silva, R., Calôba, L.P., Rebello, J.M.A, 2003: Pattern Recognition in the Automatic Inspection of Aluminium Castings. *Insight, Journal of the British Institute of Non-destructive Testing*, 45(7):441-449.

Sofia, M.; Redouane, D. (2002). Shapes recognition system applied to the non destructive testing. In *Proceedings of the 8th European Conference on Non-Destructive Testing (ECNDT 2002)*, Barcelona, 17-21 June 2002.

Silva, R.R.; Siqueira, M.H.S.; Calôba, L. P. ; da Silva, I.C. ; de Carvalho, A.A., Rebello, J.M.A. (2002). Contribution to the development of a radiographic inspection automated system. In *Proceedings of the 8th European Conference on Non-Destructive Testing (ECNDT 2002)*, Barcelona, 17-21 June 2002.

Silva, R.R.; Siqueira, M.H.S.; Calôba, L. P.; Rebello, J.M.A. (2001). Radiographic pattern recognition of welding defects using linear classifier. *Insight, Journal of the British Institute of Non-destructive Testing*, 43(10):669–674.

Wang, G.; Liao,W. (2002): Automatic Identification of different types of welding defects in radiographic images. *NDT&E International*, 35(2002):519-528.